



# Basal extrusion of single-oncogenic mutant cells induces dome-like structures with altered microenvironments

Takanobu Shirai<sup>1,2</sup> | Miho Sekai<sup>1,3</sup> | Kei Kozawa<sup>1</sup> | Nanami Sato<sup>1</sup> |  
 Nobuyuki Tanimura<sup>1</sup> | Shunsuke Kon<sup>2</sup>  | Tomohiro Matsumoto<sup>2</sup> | Takeru Murakami<sup>1</sup> |  
 Shoko Ito<sup>1,3</sup> | Andrew Tilston-Lunel<sup>4</sup> | Xaralabos Varelas<sup>4</sup> | Yasuyuki Fujita<sup>1,2</sup> 

<sup>1</sup>Department of Molecular Oncology, Graduate School of Medicine, Kyoto University, Kyoto, Japan

<sup>2</sup>Division of Molecular Oncology, Institute for Genetic Medicine, Hokkaido University Graduate School of Chemical Sciences and Engineering, Sapporo, Japan

<sup>3</sup>KAN Research Institute, Inc., Kobe, Japan

<sup>4</sup>Department of Biochemistry, Boston University School of Medicine, Boston, Massachusetts, USA

## Correspondence

Yasuyuki Fujita, Department of Molecular Oncology, Graduate School of Medicine, Kyoto University, Kyoto 606-8501, Japan.  
 Email: [fujita@monc.med.kyoto-u.ac.jp](mailto:fujita@monc.med.kyoto-u.ac.jp)

## Funding information

Shiseido Female Researcher Science Grant; Mitsubishi Foundation; SAN-ESU GIKEN CO. LTD; Takeda Science Foundation; Japan Science and Technology Agency (JST), Grant/Award Number: JPMJPS2022; JSPS Bilateral Joint Research Projects (The Royal Society) JPJSBP1, Grant/Award Number: 20K21411 and 20215703; Japan Society for the Promotion of Science (JSPS), Grant/Award Number: JP19J11375, 21H05039 and 21H05285A01; Kyoto University Live Imaging Center

## Abstract

At the initial stage of carcinogenesis, oncogenic transformation occurs in single cells within epithelial layers. However, the behavior and fate of the newly emerging transformed cells remain enigmatic. Here, using originally established mouse models, we investigate the fate of RasV12-transformed cells that appear in a mosaic manner within epithelial tissues. In the lung bronchial epithelium, most majority of RasV12-transformed cells are apically extruded, whereas noneliminated RasV12 cells are often basally delaminated leading to various noncell-autonomous changes in surrounding environments; macrophages and activated fibroblasts are accumulated, and normal epithelial cells overlying RasV12 cells overproliferate and form a convex multilayer, which is termed a 'dome-like structure'. In addition, basally extruded RasV12 cells acquire certain features of epithelial-mesenchymal transition (EMT). Furthermore, the expression of COX-2 is profoundly elevated in RasV12 cells in dome-like structures, and treatment with the COX inhibitor ibuprofen suppresses the recruitment of activated fibroblasts and moderately diminishes the formation of dome-like structures. Therefore, basal extrusion of single-oncogenic mutant cells can induce a tumor microenvironment and EMT and generate characteristic precancerous lesions, providing molecular insights into the earlier steps of cancer development.

## KEYWORDS

dome-like structure, epithelial-mesenchymal transition, initial stage of carcinogenesis, RasV12, tumor microenvironment

## 1 | INTRODUCTION

At the initial stage of carcinogenesis, oncogenic transformation occurs in single cells within epithelial layers, although the behavior and fate of the newly emerging transformed cells have not been

extensively studied yet and still remain elusive. To unravel this black box in cancer biology, mouse models have been established in which expression of an oncoprotein, such as RasV12, can be induced in a mosaic manner within a variety of epithelial tissues.<sup>1,2</sup> Previous studies have demonstrated that most RasV12-transformed cells are

**Abbreviations:** COX-2, cyclooxygenase-2; EMT, epithelial-mesenchymal transition; TME, tumor microenvironment.

Takanobu Shirai and Miho Sekai contributed equally to this work.

This is an open access article under the terms of the [Creative Commons Attribution-NonCommercial-NoDerivs](https://creativecommons.org/licenses/by-nc-nd/4.0/) License, which permits use and distribution in any medium, provided the original work is properly cited, the use is non-commercial and no modifications or adaptations are made.

© 2022 The Authors. *Cancer Science* published by John Wiley & Sons Australia, Ltd on behalf of Japanese Cancer Association.

apically extruded from epithelial monolayers and eventually eliminated from tissues.<sup>1-4</sup> These results imply a notion that the epithelium has an anti-tumor activity that does not involve immune cells; this process is termed epithelial defense against cancer (EDAC).<sup>5,6</sup> Various environmental factors that are associated with tumorigenesis such as obesity and inflammation diminish EDAC.<sup>2,7</sup> However, the fate of transformed cells that are not extruded by EDAC remains unknown.

It has been reported that at the mid or late stage of carcinogenesis, cancer cells often recruit a variety of cells including fibroblasts and immune cells and alter their properties, leading to the formation of a TME.<sup>8-11</sup> In turn, the accumulated tumor-associated stromal cells secrete various soluble factors that promote cancer progression. It is generally conceived that the formation of the TME is a chronic process that would take several months or years, often inducing pro-tumorigenic effects. Epithelial-mesenchymal transition is another important process for tumor development; epithelial cells lose cell-cell contacts and acquire mesenchymal cell states.<sup>12-17</sup> However, it remains obscure whether and how TME and EMT contribute to the very early stage of carcinogenesis.

## 2 | MATERIALS AND METHODS

### 2.1 | Antibodies and materials

Chicken anti-GFP (ab13970), rabbit anti-COX-2 (ab15191), rabbit anti-Ki-67 (ab16667), rabbit anti-mannose receptor (CD206) (ab64693), chicken anti-vimentin (ab24525), and fluorescein isothiocyanate (FITC)-conjugated goat anti-GFP (ab6662) antibodies were obtained from Abcam. Rat anti-E-cadherin (M108) antibody was purchased from Takara Bio. Rabbit anti-laminin (L9393), rabbit anti- $\alpha$ -catenin (C2081), rabbit anti-calcitonin gene-related peptide (CGRP) (C8198), and Cy3-conjugated mouse anti- $\alpha$ -SMA (C6198) antibodies were obtained from Sigma-Aldrich. Rabbit anti-keratin 5 (905504), Armenian hamster anti-CD11c (117302), rat anti-F4/80 (123102), Armenian hamster anti-CD3 $\epsilon$  (100302), rat anti-CD11b (101201), rat anti-Gr-1 (108401), rat anti-B220 (103201), and allophycocyanin (APC)-conjugated mouse anti-CD45.2 (109814) antibodies were purchased from BioLegend. Mouse anti-FOXJ1 (14-9965-82), rabbit anti-ZO-1 (61-7300), and APC-conjugated rat anti-EpCAM (17-5791-80) antibodies were purchased from Thermo Fisher Scientific. Rabbit anti-Clara cell secretory protein (Scgb1a1) (07-623) antibody was obtained from Merck Millipore. Mouse anti-p63 (ACR163) antibody was purchased from Biocare Medical. Rat anti-cytokeratin 8 (TROMA-I) antibody was obtained from Developmental Studies Hybridoma Bank. Alexa Fluor-488- and -568-conjugated anti-chicken secondary antibodies were purchased from Abcam, and Alexa Fluor-568- and -647-conjugated anti-mouse, anti-rabbit, and anti-rat secondary antibodies were obtained from Life Technologies. Hoechst 33342 stain (Thermo Fisher Scientific, H3570) was used at a dilution of 1:5000 for immunohistochemistry. The COX inhibitor ibuprofen sodium salt (#11892) was obtained from Sigma-Aldrich.

### 2.2 | Mice

*Cytokeratin19* (CK19)-Cre<sup>ERT2</sup> mice<sup>18</sup> were crossed with R26R-loxP-STOP-loxP-eYFP mice<sup>19</sup> or DNMT1-CAG-loxP-STOP-loxP-HRas<sup>V12</sup>-IRES-eGFP mice<sup>1</sup> to generate CK19-YFP mice or CK19-RasV12-GFP mice, respectively. *Scgb1a1*-Cre<sup>ERT</sup> mice<sup>20</sup> were crossed with R26R-loxP-STOP-loxP-eYFP mice or DNMT1-CAG-loxP-STOP-loxP-HRas<sup>V12</sup>-IRES-eGFP mice to generate *Scgb1a1*-YFP mice or *Scgb1a1*-RasV12-GFP mice, respectively. Mice heterozygous for each transgene were used for experiments. For PCR genotyping of mice, primers listed in Table S1 were used. CK19-YFP and CK19-RasV12-GFP mice were given a single intraperitoneal injection of 2.0 mg of tamoxifen in corn oil (Sigma-Aldrich) and were then sacrificed at the indicated times except in Figure S1(F) in which 0.1 mg of tamoxifen was administered for CK19-YFP mice. *Scgb1a1*-YFP or *Scgb1a1*-RasV12-GFP mice were given a single intraperitoneal injection of 0.1 mg or 2.0 mg of tamoxifen in corn oil respectively and were then sacrificed at the indicated times. To examine the effect of ibuprofen, the CK19-RasV12-GFP mice were pre-treated with 1.0 mg/ml of ibuprofen sodium salt in their drinking water for 3 days. Subsequently, the mice were injected intraperitoneally with 2.0 mg of tamoxifen and sacrificed 2 weeks later; ibuprofen was administered continuously during this period.

### 2.3 | Immunohistochemistry

For analyses of the lung, pancreas, and mammary gland, mice were perfused with 1% paraformaldehyde (PFA) (Sigma-Aldrich) in phosphate-buffered saline (PBS). The isolated tissues were fixed with 1% PFA in PBS for 24 h and incubated in 10% sucrose/PBS for 6 h, followed by a 1-day incubation in 20% sucrose/PBS at 4°C. The tissues were embedded in FSC 22 Clear Frozen Section Compound (Leica Biosystems) or optimal cutting temperature compound (SAKURA). Next, 10- $\mu$ m-thick frozen sections were cut using a cryostat except in Figure S1(F) in which 50- $\mu$ m-thick sequential sections were cut. The sections were incubated with 1 $\times$  Block-Ace (DS Pharma Biomedical) and 0.1% Triton X-100 for 1 h, followed by incubation with primary or secondary antibody diluted in PBS containing 0.1 $\times$  Block-Ace and 0.1% Triton X-100 for 2 h or 1 h, respectively, at room temperature. For staining *Scgb1a1* and *Foxj1*, the cut sections were incubated in citrate buffer (pH 6.0) at 90°C for 1 min using a microwave. The sections were then incubated as described above. For staining CD11b, CD11c, F4/80, Gr-1, B220, CD3 $\epsilon$ , and CD206, sections were incubated with 1 $\times$  Block-Ace without Triton X-100 followed by incubation with primary or secondary antibody diluted in PBS containing 0.1 $\times$  Block-Ace without Triton X-100. All primary antibodies were used at 1:100, except anti-GFP (1:500), FITC-conjugated anti-GFP (1:500), anti-E-cadherin (1:500), anti-laminin (1:500), anti-*Scgb1a1* (1:500), anti-keratin 5 (1:500), anti-Ki-67 (1:500), APC-conjugated anti-CD45.2 (1:500), Cy3-conjugated anti- $\alpha$ -SMA (1:500), anti-COX-2 (1:500), anti-vimentin

(1:500), APC-conjugated anti-EpCAM (1:500), anti-ZO-1 (1:500), anti-cytokeratin 8 (1:300), anti-FOXJ1 (1:400), anti- $\alpha$ -catenin (1:1000), and anti-CGRP (1:1500) antibodies. All secondary antibodies were used at 1:500. In the lung, distal bronchial epithelia were mainly analyzed in this study. For phenotype analyses of YFP or RasV12 clusters, a group of cells as well as single cells were counted as a cluster. For quantification of the number of YFP or RasV12 clusters per duct, YFP or RasV12 clusters in ducts were counted from three sequential 50- $\mu$ m-thick sections. For quantification of the size of the dome-like structures, we measured the length of a straight line linking both bottom ends of the bump of epithelia. For phenotype analyses of epithelial cells or stromal cells around YFP or RasV12 cells at 2 weeks after tamoxifen injection, cells within 60  $\mu$ m from the center of a YFP or RasV12 cluster, which was approximately the median size of dome-like structures at 2 weeks, were analyzed. For quantification of vimentin<sup>+</sup> E-cadherin<sup>-</sup> basally extruded RasV12 cells at dome-like structures, we analyzed RasV12 cells basally delaminated from the epithelial layer. Immunohistochemistry images were acquired using an Olympus FV1000 or FV1200 microscope with the Olympus FV10-ASW software or ZEISS LSM700 systems with the ZEISS ZEN software. Images were quantified using MetaMorph software (Molecular Devices) or Image J software.

## 2.4 | Statistics and reproducibility

Statistical analyses were performed with GraphPad Prism 7. To compare the difference between two groups, unpaired two-tailed Student's *t*-test or Mann-Whitney test was performed to determine *p*-values. For multiple comparisons, one-way ANOVA with Tukey's test or Kruskal-Wallis test followed by Dunn's multiple comparison test were performed to determine *p*-values. For correlation analysis, Pearson *r* and *p*-values were used to detect correlations. A *p*-value < 0.05 was considered significant. No statistical method was used to predetermine sample size.

## 3 | RESULTS

### 3.1 | Formation of dome-like structures around basally extruded RasV12-transformed cells in the bronchial epithelium

To examine how oncogenic transformation influences epithelial tissues at the initial stage of carcinogenesis, we tracked the fate of RasV12-transformed cells within various epithelial tissues. To this end, we crossed an *LSL-RasV12-IRES-eGFP* mouse with a *Cytokeratin 19 (CK19)* (epithelial-specific marker)-*Cre-ERT2* mouse whereby RasV12 expression is induced in CK19-expressing epithelial cells in a Cre-dependent fashion and traced by simultaneous expression of eGFP (Figure 1A). Administration of a low dose of tamoxifen induces infrequent recombination events, resulting

in the expression of RasV12 in a mosaic manner within a variety of epithelial tissues.<sup>2</sup> As control, we used a *Cytokeratin 19 (CK19)-Cre-ERT2; LSL-eYFP* (CK19-YFP) mouse in which eYFP alone is expressed (Figure 1A). Using these mouse models, we analyzed the phenotype of RasV12-expressing cells in the pancreas, mammary gland, and lung. At 3 days or 1 week after the tamoxifen treatment, a large fraction of RasV12-expressing cells was apically extruded or extruding from the epithelial monolayer, whereas YFP-expressing cells remained within the epithelium (Figure 1B,C and Figure S1A-E). In the ductal epithelium of the pancreas or mammary gland, at 2 weeks or 1 month, apical extrusion of RasV12 cells still continued, with very few basally extruded RasV12 cells observed (Figure S1C,E). In contrast, in the bronchial epithelium of the lung, at 2 weeks or 1 month, apical extrusion continued, but basally extruded RasV12 cells were frequently observed (Figure 1B,C). The number of RasV12 cell clusters decreased over time (Figure S1F). We did not observe the overgrowth of apically extruded cells, and the number of apically extruded RasV12 cell clusters decreased at 2 weeks and 1 month (Figure 1C and Figure S1F), suggesting that apically extruded RasV12 cells were cleared off from the epithelium. In addition, we observed that basally extruded RasV12 cells often resided under a bumped epithelial layer, which we termed a 'dome-like structure' (Figure 1B-E and Figure S1A). At 2 weeks of the tamoxifen treatment, a bumped epithelial layer was rarely observed around RasV12 cells remaining within the epithelium (no obvious dome-like structures around 72 nonextruded RasV12 cells from three mice). In contrast, ~50% of the basally extruded RasV12 cells resided within the dome-like structures (Figure 1C), suggesting that the basal extrusion of RasV12 cells could cause the formation of dome-like structures. A similar dome-like structure was also detected in the pancreas or mammary gland, but was present less frequently (Figure 1D and Figure S1C,E,G). As shown in Figure 1(C), in the control mice, at 3 days after the tamoxifen treatment, all YFP-positive cells remained within the bronchial epithelium or underwent apical extrusion, and no YFP-positive cells were found in the underlying matrix, indicating that the CK19-promoter-mediated expression was induced exclusively within the epithelial layer. In addition, previous studies have demonstrated that a Ras mutation alone is not sufficient to induce the metastatic phenotype,<sup>21,22</sup> therefore it is unlikely that RasV12 cells in the dome-like structures have been metastasized from the other tissues just after 2 weeks of RasV12 induction. Moreover, we captured several images showing that RasV12 cells were basally extruding from the epithelium (Figure S1H). Collectively, these results implied that most, if not all, of RasV12 cells in the dome-like structures originated from the overlying bronchial epithelium. In the dome-like structure, the overlying epithelium partially lacked the basement membrane component laminin (Figure 1E), suggesting an invasive property of basally extruded RasV12 cells. The size of dome-like structures gradually increased from 1 week to 1 month (Figure S1I), accompanied by the slow growth of RasV12 cell clusters within the structures (Figure S1J). Collectively, these data suggested that basally extruded RasV12-transformed cells

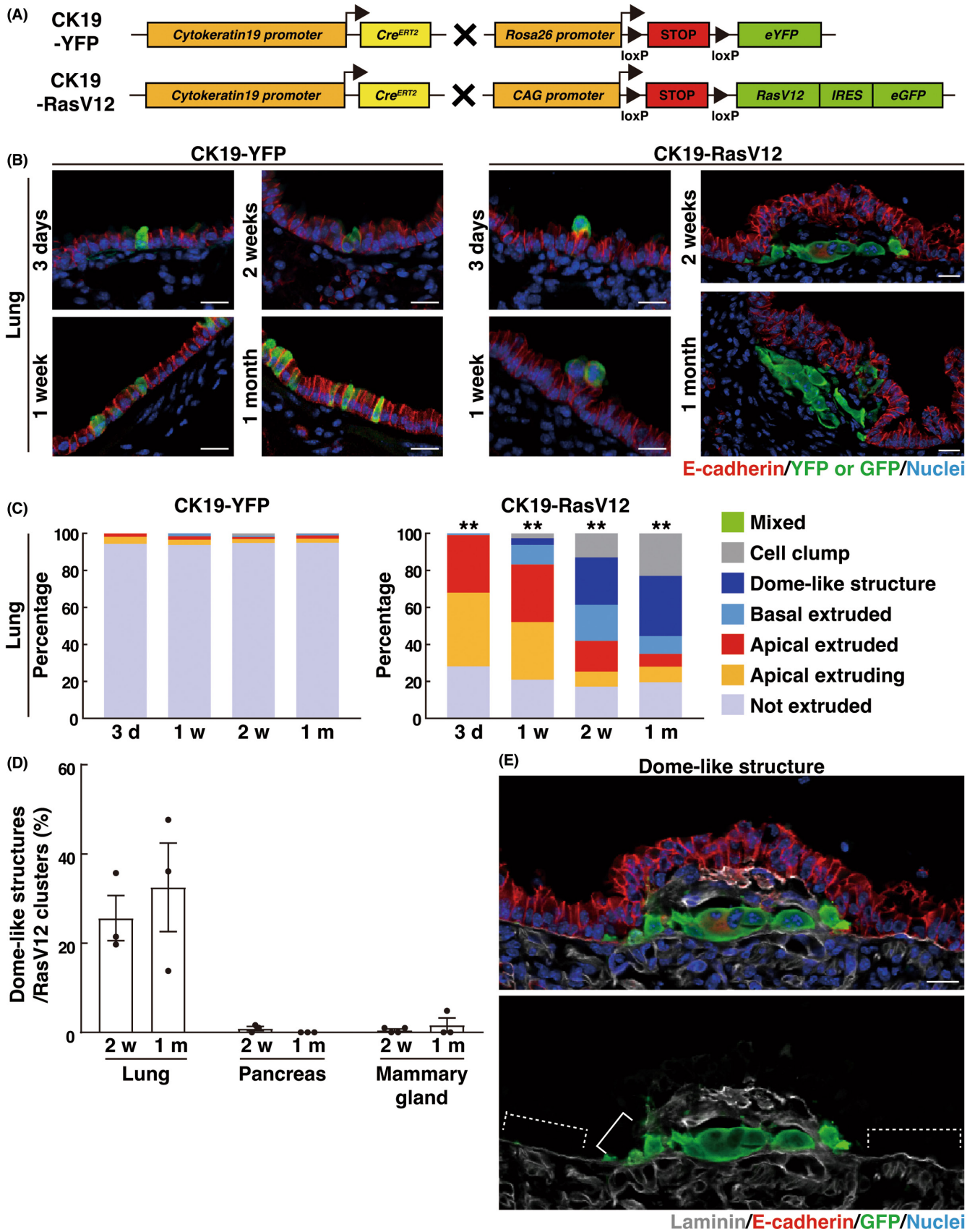


**FIGURE 1** Formation of dome-like structures around basally extruded RasV12-transformed cells in the bronchial epithelium. (A) Strategy for the establishment of the mouse model. (B) Immunofluorescence images of bronchial epithelia from CK19-YFP or CK19-RasV12 mice after tamoxifen injection. Scale bars, 20  $\mu\text{m}$ . (C) Quantification of the phenotypes of YFP or RasV12 cells in the lung.  $n = 317$  (3 days), 321 (1 week), 301 (2 weeks), and 413 (1 month) clusters for CK19-YFP.  $n = 340$  (3 days), 330 (1 week), 178 (2 weeks), and 216 (1 month) clusters for CK19-RasV12. Data are from three (3 days, 1, and 2 weeks in CK19-YFP; 2 weeks and 1 month in CK19-RasV12) or four (1 m in CK19-YFP; 3 days and 1 week in CK19-RasV12) mice. Note that the distribution of the phenotypes is compatible between mice.  $**p < 0.01$ , chi-squared test. (D) Quantification of the ratio of dome-like structures in RasV12 clusters. Data are mean  $\pm$  SEM  $n = 178$  (2 weeks) and 216 (1 month) clusters for lung from three mice.  $n = 241$  (2 weeks) and 294 (1 month) clusters for pancreas from three mice.  $n = 421$  (2 weeks) and 260 (1 month) clusters for mammary gland from four (2 weeks) and three (1 month) mice. (E) Immunofluorescence images of the dome-like structure in a CK19-RasV12 mouse at 2 weeks after tamoxifen injection. Solid and dashed lines indicate laminin-negative disrupted and laminin-positive intact basement membranes, respectively. Scale bar, 20  $\mu\text{m}$ .

could induce specific morphological alterations in the bronchial epithelial layer.

### 3.2 | Characterization of surrounding cells in dome-like structures

We further characterized the RasV12-driven dome-like structures in the bronchial epithelium. We first realized that the overlying, bumped epithelium often formed a multilayered architecture with perturbed localization of a tight junction protein ZO-1 (Figure 2A,B). We then examined the Ki-67-positive ratio of RasV12 cells and the surrounding normal epithelial cells to analyze cell proliferation. Compared with YFP-expressing control cells, RasV12 cells remaining within the epithelium had the increased Ki-67-positive ratio, and the Ki-67-positive ratio of RasV12 cells in the dome-like structures was also slightly elevated, but to a much lesser extent (Figure 2C,D). Regarding the surrounding normal epithelial cells, in the overlying, bumped epithelium of the dome-like structures, the Ki-67-positive ratio was elevated, compared with that of normal epithelial cells surrounding not-extruded YFP or RasV12 cells (Figure 2C,D), suggesting the increased cell proliferation in the multilayered epithelium within the dome-like structures. Furthermore, stromal cells accumulated around basally extruded RasV12 cells (Figure 2A, arrowheads). Immunofluorescence analyses revealed that  $\alpha$ -smooth muscle actin (SMA)-positive activated fibroblasts and CD45-positive immune cells accumulated in dome-like structures at 2 weeks after the tamoxifen treatment (Figure 2E–H). Among immune cells, the accumulation of CD11b- and/or F4/80-positive macrophages, especially CD11c-positive, CD206-negative M1 pro-inflammatory macrophages, was frequently observed, whereas F4/80-positive, CD206-positive tissue-resident alveolar macrophages, Gr-1-positive neutrophils, B220-positive B lymphocytes, or CD3 $\epsilon$ -positive T lymphocytes were absent within the dome-like structures (Figure S2A,B). At 1 month, neutrophils also accumulated around basally extruded RasV12 cells (Figure S2C), suggesting the progression of inflammatory responses. Correlation analyses revealed that the size of dome-like structures correlated with the number of either  $\alpha$ -SMA-positive cells or CD45-positive cells (Figure S2D,E).

### 3.3 | Formation of dome-like structures from Scgb1a1-expressing club cells

The bronchial epithelium consists of specialized cell types including club cells, ciliated cells, neuroendocrine cells, and basal cells, each of which expresses a specific marker protein Scgb1a1, Foxj1, CGRP and p63 (or Krt5), respectively.<sup>23</sup> In CK19-YFP mice, expression of YFP was primarily induced in Scgb1a1-positive club cells or Foxj1-positive ciliated cells (Figure 3A,B). In CK19-RasV12 mice, the proportion of GFP-labeled Scgb1a1- or Foxj1-positive cells decreased over time, suggesting that RasV12 expression induces a loss of these differentiation markers (Figure 3A,B). We cannot exclude the possibility that double-negative (Scgb1a1<sup>-</sup> and Foxj1<sup>-</sup>) RasV12 cells might outcompete Scgb1a1<sup>+</sup> or Foxj1<sup>+</sup> RasV12 cells, although dead or extruded Scgb1a1<sup>+</sup> or Foxj1<sup>+</sup> RasV12 cells were rarely observed around double-negative RasV12 cells. In contrast, very few YFP- or RasV12-expressing cells were positive for CGRP, p63 or Krt5 (Figure S3A–F). By crossing an *Scgb1a1-Cre-ERT2* mouse with an *LSL-RasV12-IRES-eGFP* mouse, we induced RasV12 expression specifically in club cells (Figure 3C) and found that the comparable dome-like structures were formed around basally extruded RasV12 cells (Figure 3D,E), indicating that dome-like structures can be derived from club cells. From 2 weeks to 3 months after tamoxifen administration, some of dome-like structures showed rapid expansion (Figure 3F,G), representing their potential to be precancerous lesions.

### 3.4 | EMT-like features in basally extruded RasV12 cells in dome-like structures

We also found that in RasV12 cells within dome-like structures, the membrane localization of prototype epithelial marker proteins E-cadherin and EpCAM was substantially diminished, whereas the expression of a mesenchymal marker vimentin was profoundly elevated, presenting some features of EMT (Figure 4A–C and Figure S4A); ~75% of basally extruded RasV12 cells were vimentin-positive and E-cadherin-negative in dome-like structures (Figure 4D). The vimentin-positive ratio of basally extruded RasV12 cells that had not formed dome-like structures was almost compatible with that of RasV12 cells in dome-like structures

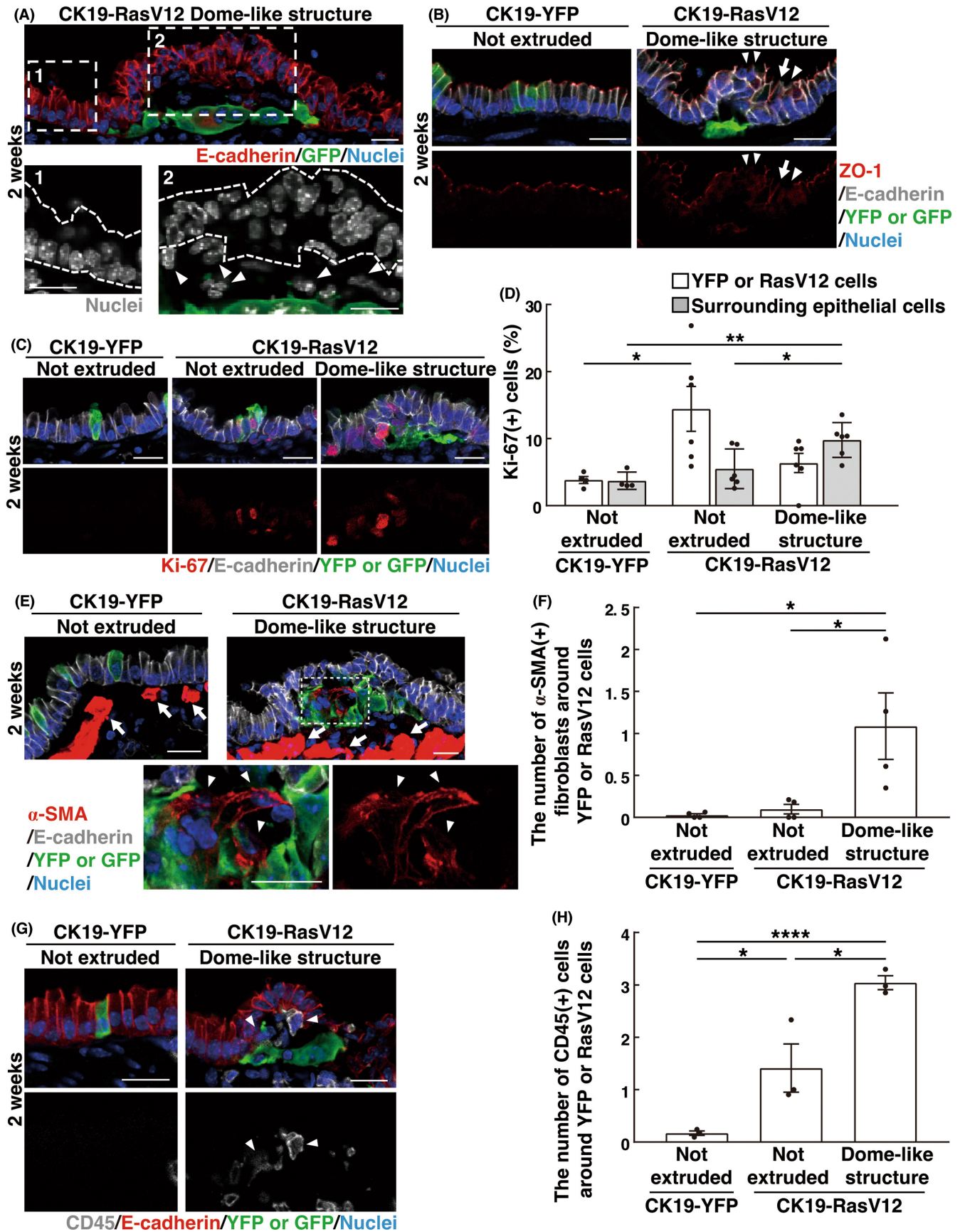


**FIGURE 2** Characterization of surrounding cells in dome-like structures. (A–C, E, G) Immunofluorescence images of dome-like structures at 2 weeks after tamoxifen injection. Scale bars, 20  $\mu\text{m}$ . (A) The multilayered epithelium overlying basally extruded RasV12-transformed cells. The dotted areas are shown at higher magnification in the lower panels. Dashed lines indicate the epithelium outside (1) or inside (2) the dome-like structure. Arrowheads indicate stromal cells within the dome-like structure. (B) Disrupted tight junctions in the overlying epithelium. Arrowheads or arrows indicate regions where tight junctions are absent or elongated, respectively. (C, D) Increased cell proliferation in the overlying epithelium within dome-like structures. (D) Quantification of the Ki-67-positive epithelial cells. Data are mean  $\pm$  SEM  $n = 222$  (not-extruded YFP), 191 (not-extruded RasV12), and 222 (RasV12 in dome-like structures) cells from four CK19-YFP or five CK19-RasV12 mice.  $n = 1124$  (surrounding not-extruded YFP), 1270 (surrounding not-extruded RasV12), and 1708 (surrounding RasV12 in dome-like structures) cells from four CK19-YFP or six CK19-RasV12 mice.  $*p < 0.05$ ,  $**p < 0.01$ , one-way ANOVA with Tukey's test. (E, F) Accumulation of activated fibroblasts in dome-like structures. (E) The dotted area is shown at higher magnification in the lower panels. Arrowheads indicate  $\alpha$ -SMA-positive activated fibroblasts within the dome-like structure, whereas arrows indicate  $\alpha$ -SMA-positive smooth muscle underneath the epithelium. Note that smooth muscle has much higher  $\alpha$ -SMA expression compared with activated fibroblasts. (F) Quantification of  $\alpha$ -SMA<sup>+</sup> fibroblasts around YFP or RasV12 cells. Data are mean  $\pm$  SEM  $n = 89$  (not extruded in CK19-YFP), 77 (not extruded in CK19-RasV12), and 107 (dome-like structure in CK19-RasV12) areas from four mice.  $*p < 0.05$ , one-way ANOVA with Tukey's test. (G, H) Accumulation of immune cells in dome-like structures. (G) Arrowheads indicate CD45-positive immune cells within the dome-like structure. (H) Quantification of CD45<sup>+</sup> cells around YFP or RasV12 cells. Data are mean  $\pm$  SEM  $n = 89$  (not extruded in CK19-YFP), 39 (not extruded in CK19-RasV12), and 99 (dome-like structure in CK19-RasV12) areas from three mice.  $*p < 0.05$ ,  $****p < 0.001$ , one-way ANOVA with Tukey's test.

(Figure 4C), whereas these expression changes were not observed in apically extruded cells (Figure S4B), suggesting that the process of basal extrusion, not of apical extrusion, causes the EMT-like phenotype. RasV12 cells in dome-like structures did express the luminal epithelial marker cytokeratin 8, indicating a maintenance of some epithelial traits (Figure S4C). Collectively, these data suggest that basally extruded RasV12 cells undergo partial EMT in dome-like structures.

### 3.5 | Effect of COX-2 inhibitor treatment on dome-like structures

Cyclooxygenase (COX) is one of the key mediators in inflammation that catalyzes the conversion from arachidonic acid to prostaglandins.<sup>24,25</sup> As previously reported,<sup>7</sup> the expression of COX-2 was elevated in epithelia harboring RasV12-expressing cells; in particular, RasV12 cells in dome-like structures showed profound COX-2 expression (Figure 5A,B). Treatment with the COX inhibitor ibuprofen moderately suppressed the number, but not the size of the dome-like structures (Figure 5C–E). The ibuprofen treatment did not affect the ratio of apically extruded/basally extruded phenotypes (Figure S5A,B). In addition, the ibuprofen treatment substantially diminished the number of  $\alpha$ -SMA-positive activated fibroblasts in the dome-like structures (Figure 5F,G), but did not affect proliferation of the overlying, bumped epithelial cells or the number of CD45-positive immune cells in the dome-like structures (Figure 5H,I). Therefore, the COX-2 pathway positively regulates the formation of dome-like structures.

## 4 | DISCUSSION

In this study, we demonstrate that, in the bronchial epithelium, basally extruded RasV12-transformed cells could induce the recruitment of macrophages and activated fibroblasts, leading to the

formation of specific dome-like structures. Previous studies have reported that TME is generated at the mid or late stage of carcinogenesis, but the data in this study suggest that comparable structures can be formed at an even earlier stage when transformed cells with a single-oncogenic mutation emerge in epithelial tissues. Expression of COX-2 is upregulated in RasV12 cells in dome-like structures (Figure 5A,B), and ibuprofen treatment diminishes the recruitment of activated fibroblasts (Figure 5G) and moderately suppresses the formation of dome-like structures (Figure 5D). Furthermore, the size of dome-like structures correlates with the number of either  $\alpha$ -SMA-positive cells or CD45-positive cells (Figure S2D,E). These data imply that macrophages and activated fibroblasts recruited by basally extruded RasV12 cells may play a certain role in the formation of dome-like structures. This is compatible with recent studies demonstrating that crosstalk between epithelial cells and the neighboring mesenchymal cells regulates tissue integrity in the lung epithelium.<sup>26–28</sup> The ibuprofen treatment does not affect proliferation of the overlying epithelial cells or the recruitment of immune cells in dome-like structures. Therefore, the underlying molecular mechanisms of dome-like structures remain to be elucidated.

How are dome-like structures generated preferentially in the lung, not in the pancreas or breast? Several possible mechanisms can be considered. For instance, club cells, one of the putative origins of dome-like structures, have a capacity to dedifferentiate upon insults.<sup>29</sup> An oncogenic mutation may hijack the plastic property of club cells, thereby inducing EMT. In addition, the lung epithelium is a relatively vasculature-enriched tissue with abundant capillary vessels, so that the recruitment of macrophages could be promptly facilitated by the bloodstream. These still remain speculative assumptions, therefore further research will be required to address this question.

The findings in this study also indicate a technical pitfall in the current genetic analyses targeting precancerous lesions. Recent next-generation sequencing analyses have revealed that a variety of oncogenic mutations is present in morphologically normal epithelial tissues from human patients.<sup>30–32</sup> However, in those studies,

E-cadherin- or EpCAM-positive epithelial cells are mainly analyzed. Therefore, transformed cells in dome-like structures are likely to be overlooked from those analyses. Identification of specific markers for this novel type of precancerous lesions would shed more light on

the initial stage of carcinogenesis, which is currently a black box in cancer biology.

We have examined the fate of dome-like structures up to 3 months (Figure 3F), and some of dome-like structures expanded and form a

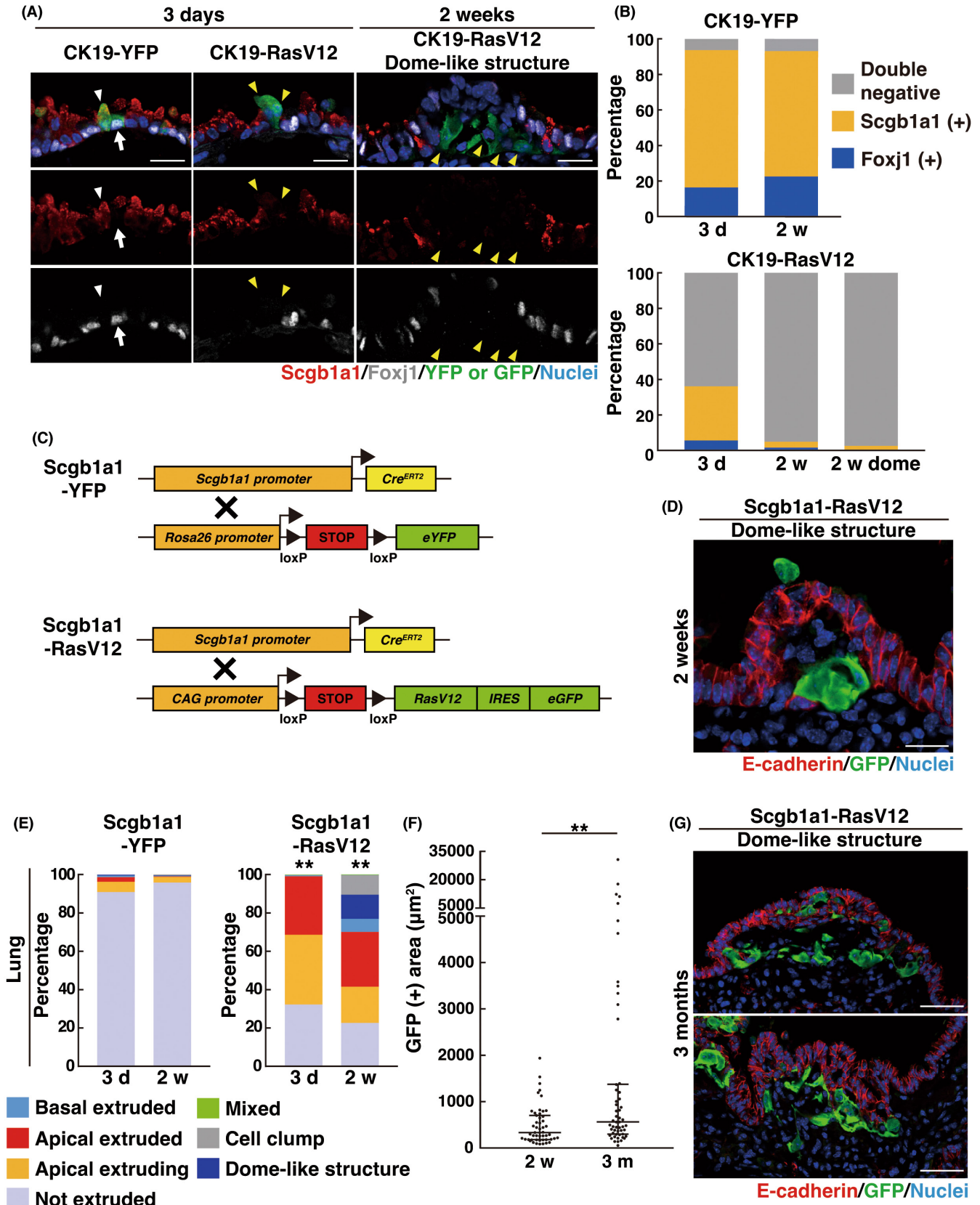




**FIGURE 3** Formation of dome-like structures in *Scgb1a1*-RasV12 mice. (A) Immunofluorescence images of bronchial epithelia from CK19-YFP or CK19-RasV12 mice with tamoxifen treatment. Scale bars, 20  $\mu\text{m}$ . (A, B) A loss of the differentiation markers in RasV12-expressing cells. (A) White arrows or arrowheads indicate YFP-expressing *Foxj1*<sup>+</sup> ciliated cells or *Scgb1a1*<sup>+</sup> club cells, respectively, whereas yellow arrowheads indicate RasV12-expressing cells lacking *Foxj1* and *Scgb1a1* expression. (B) Quantification of *Foxj1*<sup>+</sup>, *Scgb1a1*<sup>+</sup> or *Foxj1*<sup>-</sup> *Scgb1a1*<sup>-</sup> double-negative cells.  $n = 269$  (3 days) and 248 (2 weeks) cells for CK19-YFP and 285 (3 days), 305 (2 weeks), and 302 (2 weeks dome) cells for CK19-RasV12. Data are from three mice. (C) Strategy for the establishment of mice expressing YFP or RasV12-GFP under the control of a club cell-specific *Scgb1a1* promoter. (D, G) Immunofluorescence images of dome-like structures in bronchial epithelia from *Scgb1a1*-RasV12 mice at 2 weeks (D) or 3 months (G) after tamoxifen injection. Scale bars, 20  $\mu\text{m}$  (D) or 50  $\mu\text{m}$  (G). (E) Quantification of the phenotypes of YFP or RasV12 cells.  $n = 373$  (3 days) and 408 (2 weeks) clusters for *Scgb1a1*-YFP and 410 (3 days) and 407 (2 weeks) clusters for *Scgb1a1*-RasV12. Data are from four mice.  $**p < 0.01$ , chi-squared test. (F) Quantification of GFP-positive area in dome-like structures from *Scgb1a1*-RasV12 mice. Data are median  $\pm$  quartiles.  $n = 51$  (2 weeks) and 54 (3 month) dome-like structures from four (2 weeks) or three (3 months) mice.  $**p < 0.01$ , Mann-Whitney test. Note that the longer-term fate of dome-like structures can be analyzed in *Scgb1a1*-RasV12 mice, but not in CK19-RasV12 mice, as CK19-RasV12 mice die within 2 months of tamoxifen injection.

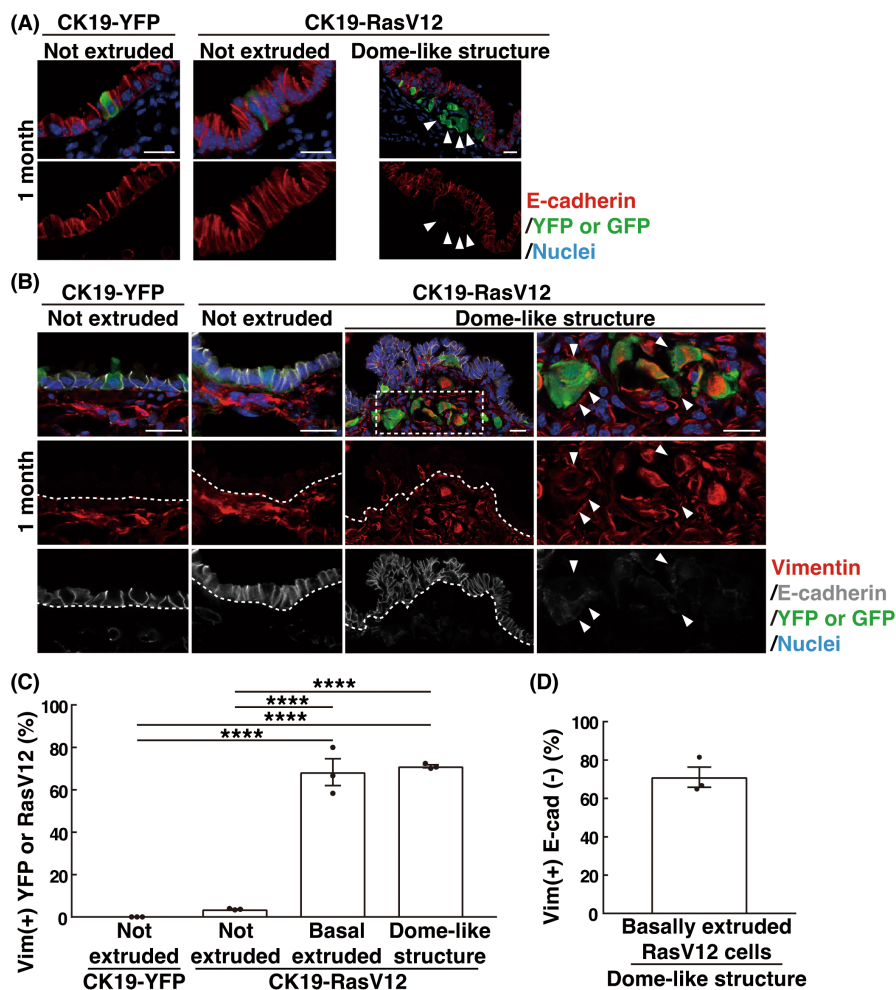


**FIGURE 4** EMT-like features in basally extruded RasV12-transformed cells in dome-like structures. (A, B) Immunofluorescence images of E-cadherin and vimentin in bronchial epithelia from CK19-YFP or CK19-RasV12 mice with tamoxifen treatment. Scale bars, 20  $\mu\text{m}$ . (A) Arrowheads indicate E-cadherin-negative basally extruded RasV12 cells in the dome-like structure. (B) Dashed lines delineate the basement membrane of the epithelial layer. The dotted area is shown at higher magnification in the right-hand panels. Arrowheads indicate vimentin-positive, E-cadherin-negative basally extruded RasV12 cells in the dome-like structure. (C, D) Quantification of vimentin<sup>+</sup> YFP or RasV12 cells (C) and vimentin<sup>+</sup> E-cadherin<sup>-</sup> basally extruded RasV12 cells (D). (C) 'Not extruded' encompasses both single and clustered nonextruded YFP or RasV12 cells; vimentin-positive ratio of 'not extruded' was low, irrespective of the number of cells in cell clusters. Data are mean  $\pm$  SEM  $n = 152$  (not extruded in CK19-YFP), 110 (not extruded in CK19-RasV12), 57 (basally extruded in CK19-RasV12), and 198 (dome-like structure in CK19-RasV12) cells from three mice.  $****p < 0.001$ , one-way ANOVA with Tukey's test. (D)  $n = 124$  cells from three mice.

tumorous mass over time (Figure 3F,G), suggesting that they could be latent precancerous lesions. It has been reported that the TME facilitates the mid or late stage of cancer development.<sup>9-11</sup> Therefore,

similarly, the accumulated immune cells or activated fibroblasts in dome-like structures may provide pro-tumorigenic effects on basally delaminated, single-oncogenic mutant cells. However, it remains

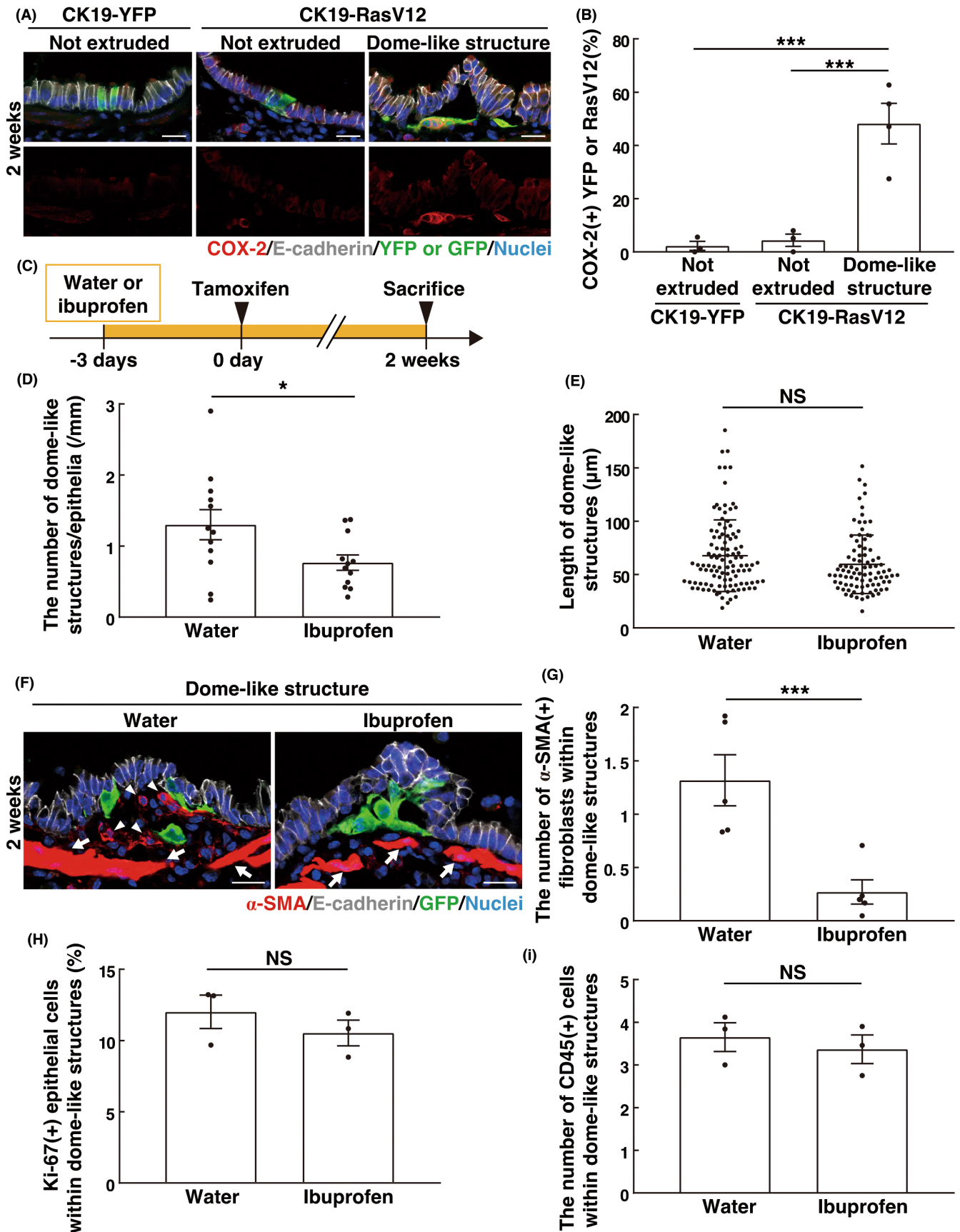


**FIGURE 5** Effect of COX-2 inhibitor treatment on dome-like structures. (A) Immunofluorescence images of COX-2 in bronchial epithelia from CK19-YFP or CK19-RasV12 mice with tamoxifen treatment. Scale bars, 20  $\mu\text{m}$ . (B) Quantification of COX-2-positive YFP or RasV12 cells. Data are mean  $\pm$  SEM  $n = 183$  (not extruded in CK19-YFP), 79 (not extruded in CK19-RasV12), and 231 (dome-like structure in CK19-RasV12) cells from three (CK19-YFP and not extruded in CK19-RasV12) or four (dome-like structure in CK19-RasV12) mice. \*\*\* $p < 0.005$ , one-way ANOVA with Tukey's test. (C) Experimental design for the ibuprofen treatment in CK19-RasV12 mice. CK19-RasV12 mice were continuously administrated with ibuprofen in drinking water starting at 3 days before tamoxifen injection and analyzed at 2 weeks. (D, E) Quantification of the effect of ibuprofen on the number (D) and length (E) of dome-like structures. (D) Data are mean  $\pm$  SEM  $n = 12$  sections from four mice. (E) Data are median  $\pm$  quartiles.  $n = 109$  (water) and 89 (ibuprofen) dome-like structures from three mice. \* $p < 0.05$ , unpaired two-tailed Student's  $t$ -test (D) or NS, not significant, Mann-Whitney test (E). (F) Immunofluorescence images of  $\alpha$ -SMA in bronchial epithelia from CK19-RasV12 mice with ibuprofen and tamoxifen treatment. Arrowheads indicate  $\alpha$ -SMA-positive activated fibroblasts within the dome-like structure, whereas arrows indicate  $\alpha$ -SMA-positive smooth muscle underneath the epithelium. Note that smooth muscle has much higher  $\alpha$ -SMA expression compared with activated fibroblasts. Scale bars, 20  $\mu\text{m}$ . (G) Quantification of the effect of ibuprofen on  $\alpha$ -SMA-positive activated fibroblasts in dome-like structures. Data are mean  $\pm$  SEM  $n = 105$  (water) and 129 (ibuprofen) dome-like structures from five mice. \*\*\* $p < 0.005$ , unpaired two-tailed Student's  $t$ -test. (H, I) Quantification of the effect of ibuprofen on Ki-67<sup>+</sup> surrounding epithelial cells (H) or CD45<sup>+</sup> immune cells (I) in dome-like structures. (H) Data are mean  $\pm$  SEM  $n = 1575$  (water) and 1301 (ibuprofen) cells from three mice. (I)  $n = 70$  (water) and 64 (ibuprofen) dome-like structures from three mice. NS, not significant, unpaired two-tailed Student's  $t$ -test.

unknown whether RasV12-transformed cells in dome-like structures will develop into malignant tumors over time. The functional significance and long-term fate of dome-like structures in cancer development need to be further explored in future studies.

#### ACKNOWLEDGMENTS

This work was also supported by Kyoto University Live Imaging Center.

#### FUNDING INFORMATION

Japan Society for the Promotion of Science (JSPS) grant-in-aid for scientific research on innovative areas 21H05285A01, grant-in-aid for scientific research (S) 21H05039, JSPS Bilateral Joint Research Projects (The Royal Society) JPJSBP1 20215703, JSPS grant-in-aid for challenging research (Pioneering) 20K21411, Japan Science and Technology Agency (JST) (Moonshot R&D: grant number JPMJPS2022), the Takeda Science Foundation, and SAN-ESU GIKEN CO. LTD (to YF), grant-in-aid for JSPS Research Fellow JP19J11375 (to TS), Mitsubishi Foundation and Shiseido Female Researcher Science Grant (to MS).

#### CONFLICT OF INTEREST

Dr. Fujita received honoraria from Eisai Co, Ltd and research expenses from Eisai Co, Ltd. The other authors have no conflict of interest.

#### DATA AVAILABILITY STATEMENT

The data that support the findings of this study are available from the corresponding author upon reasonable request.

#### ANIMAL STUDIES

All animal experiments were conducted under the guidelines of the Animal Care Committee of Kyoto University. The animal protocols were reviewed and approved by the Kyoto University Animal Care Committee (approval no.: Med Kyo 22056).

#### ORCID

Shunsuke Kon  <https://orcid.org/0000-0002-2693-6128>

Yasuyuki Fujita  <https://orcid.org/0000-0002-5875-7052>

#### REFERENCES

- Kon S, Ishibashi K, Katoh H, et al. Cell competition with normal epithelial cells promotes apical extrusion of transformed cells through metabolic changes. *Nat Cell Biol.* 2017;19:530-541.
- Sasaki A, Nagatake T, Egami R, et al. Obesity suppresses cell-competition-mediated apical elimination of RasV12-transformed cells from epithelial tissues. *Cell Rep.* 2018;23:974-982.
- Brown S, Pineda CM, Xin T, et al. Correction of aberrant growth preserves tissue homeostasis. *Nature.* 2017;548:334-337.
- Hill, W., Zaragkoulias, A., Salvador-Barbero, B. et al. EPHA2-dependent outcompetition of KRASG12D mutant cells by wild-type neighbors in the adult pancreas. *Curr Biol* 2021; 31: 2550-2560.e5.
- Kajita M, Sugimura K, Ohoka A, et al. Filamin acts as a key regulator in epithelial defence against transformed cells. *Nat Commun.* 2014;5:4428.
- Kon S, Fujita Y. Cell competition-induced apical elimination of transformed cells, EDAC, orchestrates the cellular homeostasis. *Dev Biol.* 2021;476:112-116.
- Sato N, Yako Y, Maruyama T, et al. The COX-2/PGE2 pathway suppresses apical elimination of RasV12-transformed cells from epithelia. *Commun Biol.* 2020;3:132.
- Quail DF, Joyce JA. Microenvironmental regulation of tumor progression and metastasis. *Nat Med.* 2013;19:1423-1437.
- Whiteside TL. The tumor microenvironment and its role in promoting tumor growth. *Oncogene.* 2008;27:5904-5912.
- Hinshaw DC, Shevde LA. The tumor microenvironment innately modulates cancer progression. *Cancer Res.* 2019;79:4557-4566.
- Hanahan D, Coussens LM. Accessories to the crime: functions of cells recruited to the tumor microenvironment. *Cancer Cell.* 2012;21:309-322.
- Dongre A, Weinberg RA. New insights into the mechanisms of epithelial-mesenchymal transition and implications for cancer. *Nat Rev Mol Cell Biol.* 2019;20:69-84.
- Yang J, Antin P, Berx G, et al. Guidelines and definitions for research on epithelial-mesenchymal transition. *Nat Rev Mol Cell Biol.* 2020;21:341-352.
- Kalluri R, Weinberg RA. The basics of epithelial-mesenchymal transition. *J Clin Invest.* 2009;119:1420-1428.
- Nieto MA, Huang RY, Jackson RA, Thiery JP. EMT: 2016. *Cell.* 2016;166:21-45.
- Derynck R, Weinberg RA. EMT and cancer: more than meets the eye. *Dev Cell.* 2019;49:313-316.
- Brabletz T, Kalluri R, Nieto MA, Weinberg RA. EMT in cancer. *Nat Rev Cancer.* 2018;18:128-134.
- Means AL, Xu Y, Zhao A, Ray KC, Gu G. A CK19(CreERT) knockin mouse line allows for conditional DNA recombination in epithelial cells in multiple endodermal organs. *Genesis.* 2008;46:318-323.

19. Srinivas S, Watanabe T, Lin CS, et al. Cre reporter strains produced by targeted insertion of EYFP and ECFP into the ROSA26 locus. *BMC Dev Biol.* 2001;1:4.
20. Rawlins EL, Okubo T, Xue Y, et al. The role of Scgb1a1+ Clara cells in the long-term maintenance and repair of lung airway, but not alveolar, epithelium. *Cell Stem Cell.* 2009;4:525-534.
21. Jackson EL, Willis N, Mercer K, et al. Analysis of lung tumor initiation and progression using conditional expression of oncogenic K-ras. *Genes Dev.* 2001;15:3243-3248.
22. Gidekel Friedlander SY, Chu GC, Snyder EL, et al. Context-dependent transformation of adult pancreatic cells by oncogenic K-Ras. *Cancer Cell.* 2009;16:379-389.
23. Basil MC, Katzen J, Engler AE, et al. The cellular and physiological basis for lung repair and regeneration: past, present, and future. *Cell Stem Cell.* 2020;26:482-502.
24. Turini ME, DuBois RN. Cyclooxygenase-2: a therapeutic target. *Annu Rev Med.* 2002;53:35-57.
25. Simmons DL, Botting RM, Hla T. Cyclooxygenase isozymes: the biology of prostaglandin synthesis and inhibition. *Pharmacol Rev.* 2004;56:387-437.
26. Lee, J. H., Tammela, T., Hofree, M. et al. Anatomically and functionally distinct lung mesenchymal populations marked by Lgr5 and Lgr6. *Cell* 2017; 170: 1149-1163.e12.
27. Moiseenko A, Vazquez-Armendariz AI, Kheirollahi V, et al. Identification of a repair-supportive mesenchymal cell population during airway epithelial regeneration. *Cell Rep.* 2020;33:108549.
28. Volckaert, T., Yuan, T., Chao, C. M. et al. Fgf10-Hippo epithelial-mesenchymal crosstalk maintains and recruits lung basal stem cells. *Dev Cell* 2017; 43: 48-59.e5.
29. Tata PR, Mou H, Pardo-Saganta A, et al. Dedifferentiation of committed epithelial cells into stem cells in vivo. *Nature.* 2013;503:218-223.
30. Martincorena I, Roshan A, Gerstung M, et al. Tumor evolution. High burden and pervasive positive selection of somatic mutations in normal human skin. *Science.* 2015;348:880-886.
31. Martincorena I, Fowler JC, Wabik A, et al. Somatic mutant clones colonize the human esophagus with age. *Science.* 2018;362:911-917.
32. Yokoyama A, Kakiuchi N, Yoshizato T, et al. Age-related remodeling of oesophageal epithelia by mutated cancer drivers. *Nature.* 2019;565:312-317.

#### SUPPORTING INFORMATION

Additional supporting information can be found online in the Supporting Information section at the end of this article.

**How to cite this article:** Shirai T, Sekai M, Kozawa K, et al. Basal extrusion of single-oncogenic mutant cells induces dome-like structures with altered microenvironments. *Cancer Sci.* 2022;113:3710-3721. doi: [10.1111/cas.15483](https://doi.org/10.1111/cas.15483)